JOURNAL OF MATERIALS SCIENCE **35** (2000) 6267–6275

Measurements of crack tip strain field in wood at the scale of growth rings

F. THUVANDER
Division of Polymer Engineering, Luleå University of Technology, SE-97187 Luleå, Sweden

M. SJÖDAHL
Division of Experimental Mechanics, Luleå University of Technology, SE-97187 Luleå, Sweden

L. A. BERGLUND
Division of Polymer Engineering, Luleå University of Technology, SE-97187 Luleå, Sweden
E-mail: Lars.Berglund@mb.luth.se

The fracture mechanisms of wood have often been interpreted on the scale of cell walls. Although this scale is important, the scale of growth rings needs to be considered in the same context. In the present study, the crack tip strain field of radial *TR* cracks at the scale of growth rings is measured by electronic speckle photography. The methodology is discussed in detail as well as the data reduction scheme. The tip is in the earlywood layer and the crack plane of the *TR* crack is perpendicular to the stiffer latewood layer. Increasing opening mode load is applied in-situ as the crack is observed by reflected light optical microscopy. Strains are measured on direct images of the microstucture. In contrast to some other methodologies, this allows direct correlation between strain field and microstructure. In the softer earlywood, tangential strains extend considerable distances in the tangential direction. Due to the stiff latewood, the strain is heavily constrained in the radial direction. This nature of the local strain field has been largely neglected, despite its obuius significance to *TR* crack growth mechanisms.

1. Introduction

In the present study, we measured crack tip strain fields in order to improve our understanding of crack growth in wood. Crack growth mechanisms in wood are obviously critical in load-bearing elements. Failure initiation, as well as propagation, involves crack growth through cell walls and through earlywood and latewood areas of different densities. The often quoted variability of wood failure properties is related to details in these crack growth mechanisms. Another area where crack growth concepts are helpful is in cutting processes of wood. In particular knife cutting processes essentially rely on crack growth. The knife may be pushed into the wood material where it directly cuts through cell walls. In addition, the knife provides an opening moment which may drive the crack forward, ahead of the knife edge. From the point of view of industrial cutting processes, it would often be advantageous if crack growth was stable, controlled and with a straight crack path in one plane. The resulting fracture surface would be smooth and planar on the macroscopic scale. Since this scenario corresponds to a minimum of cell wall damage at the surface and in the underlying material, the energy required for the cutting process would be small. This is also beneficial in the context of adhesive bonding or paint treatment of the surface. The reason is that adhesion of paint or an adhesive is improved with decreasing surface and subsurface damage. Although our preference is for stable crack growth with smooth crack surfaces, experimental data unfortunately often demonstrate unstable and irregular paths of crack growth [1, 2].

Wood is a highly anisotropic material with the principal axis of anisotropy conventionally denoted, R, T and L for the radial, tangential and longitudinal direction respectively, see Fig. 1. The elastic modulus in the longitudinal direction is about one order of magnitude higher than in the other two directions. Also the fracture behaviour is linked to the material structure and eight systems of crack propagation can be identified by material symmetry [3]. Each system is commonly identified with a pair of letters, the first indicating the crack surface normal and the second describing the direction of crack growth. In the present study we are concerned with *TR* cracks. The crack grows in the radial direction, perpendicular to the alternating earlywood and latewood layers.

One example of irregular paths of crack growth is the surface roughness data measured by Engøy *et al.* [1] for *TR* crack growth. Fracture surfaces were found to have amplitudes up to 3 mm for cracks in the tangential direction over a measured length of 25.6 mm. Regarding fracture mechanisms, the cell wall level is often discussed in the literature. This is the focus of recent

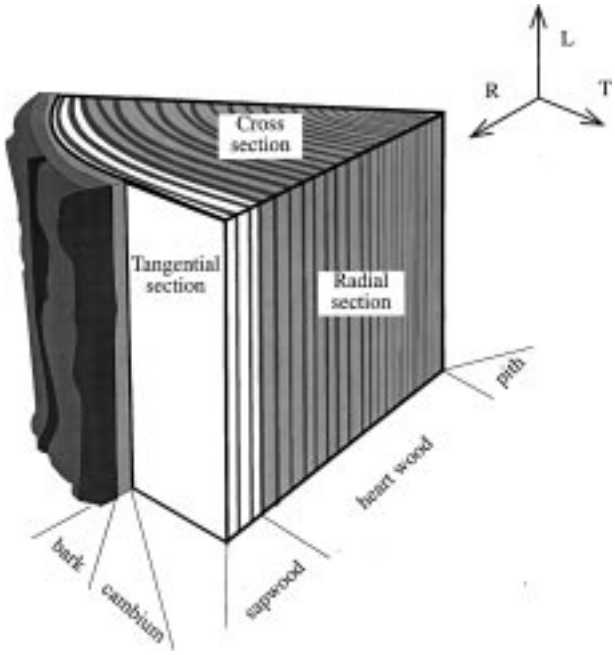

Figure 1 Axis of anisotropy, *R*, *T* and *L* for the radial, tangential and longitudinal direction respectively.

studies of longitudinal failure, relevant for *LR* fracture [4–6]. In the present study, our interest is in *TR* fracture where we focus on the scale of growth rings. Let us compare the two fracture cases of *TR* and *TL* fracture. It is interesting to note that the fracture toughness for the *TR* case is higher than for the *TL* case [7, 8]. This is despite the fact that the fracture planes are the same. The *TR* crack grows in the radial direction cutting through alternating layers of earlywood and latewood. In contrast, the front of a *TL* crack grows in the longitudinal direction so that the front is present simultaneously in both earlywood and latewood.

The crackplane is predominantly stable for *TL* cracks [9] whereas for *TR* cracks, the plane tends to deviate from its original plane during growth [2]. The crack path is dependent on the stability of crack extension. Stable cracks result primarily in separation of neighboring cells from each other whereas unstable crack growth leads to a larger proportion of crack growth through cell walls [10].

Ashby *et al*. [11] conducted an interesting experimental study of *TR* cracks by *in-situ* observations in a scanning electron microscope. Unstable crack growth was confirmed and crack jumps of several hundred cell diameters were observed. It is of interest to explain why unstable crack growth tends to occur for *TR* cracks and why the fracture toughness is higher for *TR* as compared with *TL* cracks. Not only would this improve our basic understanding of crack growth in wood but it may also be of some practical importance. Attempts to produce stable *TR* cracks resulting in smooth fracture surfaces have so far met with limited success. If this is due to fundamental difficulties, the *TL* mode of crack growth is better suited for development of new cutting technologies where a smooth fracture surface is desired.

The objective of the present set of studies is to improve the understanding of *TR* crack growth mechanisms at the growth ring scale. This was addressed by *in-situ* observations of growth mechanisms for mode I *TR* cracks [12]. It was noted that *TR* cracks often show "stick-slip" type of crack growth where the plane of crack growth is also frequently changing as the crack extends from one growth ring to another. This mechanism is likely to lead to enhanced toughness with a jagged appearance of the fracture surface. Improved knowledge of the crack tip strain field may shed some light on the observed crack growth process. In the present study, the objective is therefore to experimentally study the state of strain at the crack tip at the growth ring level in pine. Electronic speckle photography, also termed the image correlation technique, is used. The pine *Pinus sylvestris* L. samples are sapwood samples studied in the green state in order to avoid damage induced by drying. Previous studies have indicated cell wall damage as a result of drying of wood [13, 14]. Because of the anisotropy of the individual S1, S2 and S3 layers constituting the cell wall, considerable drying stresses are expected at the cell wall level [14].

2. Electronic speckle photography (ESP)

An ESP system is built from standard equipment, described in Fig. 2. A CCD-camera, connected to a PC via a frame-grabber, collects images of the random pattern present on the object. The technique relies on that the motion of this random pattern can be detected between frames, therefore the quality of the pattern is crucial. An elegant way to produce the necessary pattern is to use the so called laser speckles obtained when illuminating a diffusely reflecting object with a laser. However, using laser speckles on wood at high magnification is not convenient because of speckle decorrelation and low speckle contrast. Another method is to attach the random pattern onto the surface, for instance paint the surface with retro-reflecting paint [15], or attach carbon particles as those found in photocopy toner cartridges onto the surface [16]. In some situations it is also possible to use the surface texture itself [17]. Once at least two images of the test surface is captured, the relative displacement between them can be calculated.

In recent work by Kifetew *et al*. [13] and Thuvander *et al*. [14], it was demonstrated that drying of wood most likely leads to damage in the cell wall microstructure.

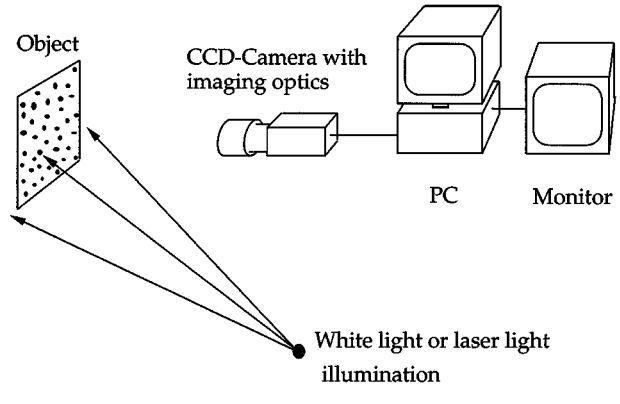

Figure 2 An Electronic speckle photography set-up.

In order to ensure that the microstructure is undamaged, the sample must therefore be kept in soaked condition during the experiment. In the soaked state the lumen cavities are filled with water. The water in the lumen makes it difficult to observe the structure and hence provide pictures with good contrast. We found that if the surface was rubbed with a slurry of talcum powder, the gray scale in the picture was broadened and picture quality was enhanced to an extent where it was possible to perform the calculation on the images.

Motion estimation is of general importance in image analysis and the various techniques used can be classified into three groups:pixel-recursive techniques (for instance optical flow), character tracking techniques (for instance particle tracking), and block-matching techniques (correlation). The various techniques within these groups have their different advantages concerning accuracy, spatial resolution, noise tolerance, and calculation efficiency. However, because of their noise tolerance and high accuracy, the block-matching techniques are often a good choice for performing high quality deformation measurements. ESP is a technique that belongs to this group. The fundamentals of the specific algorithm used here have been described in detail elsewhere [18, 19] and will therefore only be summarised here.

Consider the correlation procedure schematically described in Fig. 3. The mean displacement between the two sub-areas is given by the peak position of the spatial cross-correlation between them. The accuracy of the cross-correlation function depends on the sub-image window, the spatial frequency content in the image (i.e. the average speckle size and density), the sub-area overlap, image distortion, and speckle correlation [19]. In other words, the accuracy depends on how many speckles that can be made to overlap within the given correlation window. It is therefore advantageous to iterate the cross-correlation procedure with new choices of sub-image until the maximum overlap is found. For typical values, the present algorithm then manages to detect the displacement with a random error of 1% of the pixel pitch, which translated into object coordinates gives an accuracy of 0.1 μm at a magnification of unity. Repeating the procedure in an arbitrary number of sub-areas on the object gives the in-plane displacement field, which is visualized in Fig. 3.

From the materials point of view, the strain field rather than the displacement field is of primary interest. The most direct way to obtain the strain is through numerical differentiation of the displacement field, in the following triangular elements were used. The points of the observed displacements were considered as nodal points and the Gauss point of the triangular element was then set as the observation point for the strains. Since triangular elements were used, only three points of displacement define the state of strain. The compatibility within the element is therefore always fulfilled and the number of missing points is minimized.

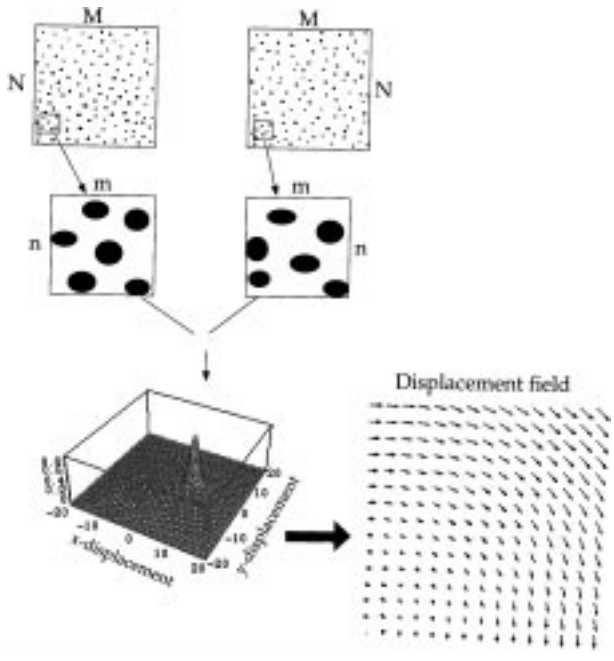

Figure 3 Principle of the correlation algorithm. Two subimages of size $m \times n$ are extracted from the full images of size $M \times N$ and are correlated. The local deformation is given by the position of the correlation peak. Repeating the procedure for new positions in the full images, gives the full displacement field.

3. Experimental procedure

From the sapwood of green pine, *Pinus sylvestris* L., blocks of dimensions $20 \times 20 \times 30$ mm were cut in the radial, tangential, and longitudinal directions of the stem respectively. To prepare the surface for the future study in the microscope, the surface was cleaned with a microtome at the axial surface to visualise the ultrastructure of the wood. A sample with a thickness of 6 mm was then cut from the square section with a sharp fine saw. Two holes were drilled for application of the load, see Fig. 4.

To enhance the contrast between the wood substance in the cell wall and the lumen for the moist green wood, a slurry of talcum powder was rubbed into the surface, thus filling the lumen with talcum slurry. The surface was then wiped clean with a piece of soft paper. The procedure of filling the lumen with talcum powder enabled us to maintain a high contrast in the picture.

A crack was introduced using a new razor blade. The sample was then mounted in a tensile testing stage, (Minimat by Polymer Labs), developed for use under a microscope. While observed under microscope, the

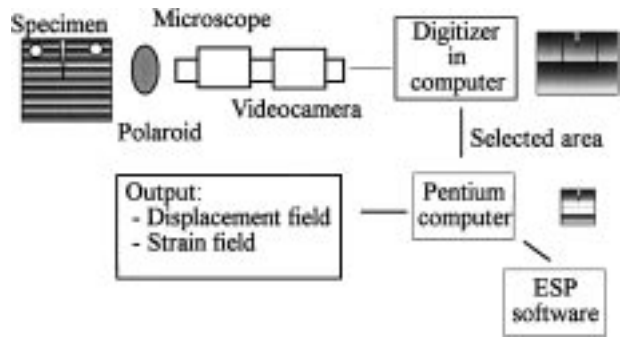

Figure 4 Schematic of the experimental procedure. From the images captured by the videocamera, an area of 512×512 pixels was selected for the analysis of the strain field.

sample was loaded under displacement control until the crack started to propagate. Under maintained displacement, the crack was allowed to propagate until it stopped. The opening displacement was then decreased until the crack was closed, so that the location of the crack at zero load was known. At the location of the crack tip, a series of images were recorded as a reference. An increase in crack opening displacement was applied to the sample in steps. At each incremental step, a series of images was acquired, averaged, and stored. The stepwise increase in opening displacement was continued until the crack propagated.

All the images were acquired from the video camera in the microscope by use of the program NIH image, shareware from the National Institute of Health. In order to decrease the noise in the video images, the pictures used for the displacement analysis were the average of 32 images taken at the same displacement. The equipment used was a Macintosh Power PC 7600 equipped with a video card. The stored images had standard video resolution (PAL) with 256 gray levels.

From the set of images, an area around the crack tip of 1.1×1.1 mm (512×512 pixels) was selected for the analysis and the strain field was calculated at five levels of crack opening displacement.

4. Results and discussion

In stress analysis of wood, the material is commonly described as a homogeneous, anisotropic material. This approach is often well motivated in mechanics analyses of structures such as beams. However, it is not sufficient if the goal is to understand structure-property relationships and failure mechanisms on the microscale. In gradually changing the scale of observation from macro- to micro-scale, it seems reasonable to choose the scale of growth rings as the first sub-scale. At this level, the dimensions of structural features are in the order of mm, perhaps down to one tenth of a mm. Although in an optical microscope individual cells are clearly observable at this level, we choose to disregard individual cells in this approach. The reason is that our analysis of the state of strain is simplified substantially if we assume that each earlywood or latewood layer is homogeneous although anisotropic. In a stress analysis, we may accomodate gradients in elastic properties at the interface between earlywood and latewood layers through the introduction of thin homogeneous layers.

There are some previously published measurements of wood displacement fields. Zink *et al*. 1995 [16] applied the technique of digital image correlation for the measurement of macroscale strain fields in wood

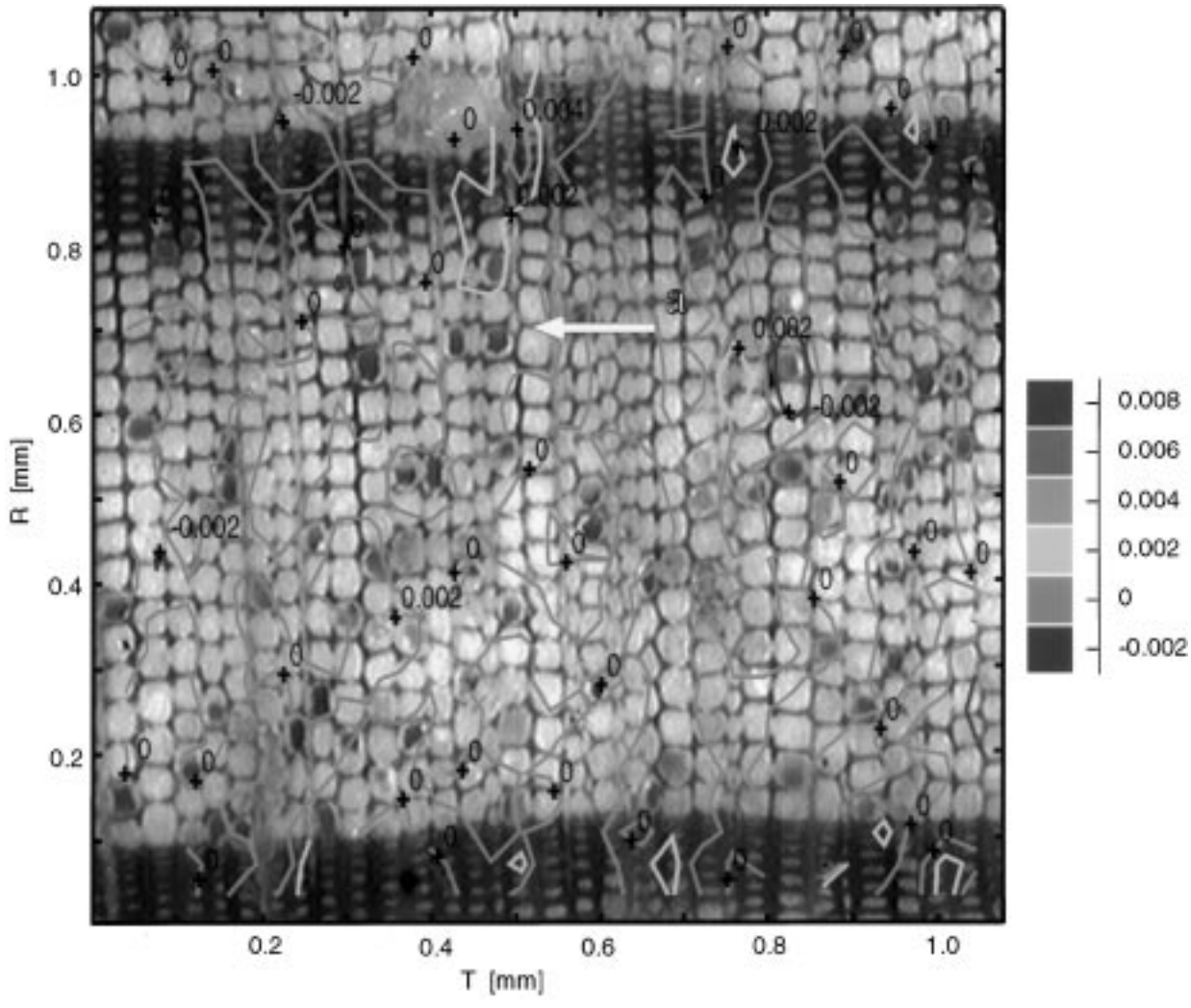

Figure 5 Crack tip at position a: The first load increment showing negligible strain levels in the overall structure. The + and the corresponding number (in dimensionless strain) mark the corresponding strain.

specimens under compression. A speckle pattern of carbon particles were applied to the surface. A related approach was adopted by Choi *et al*. [20, 21] to study the microscale failure of wood in compression from microscopy images. In the present study, rather than using an imposed pattern as was done in the references [16, 20, 21], we use the structure of wood itself in our measurements. This allows us to directly correlate the measured strain field with the wood microstructure.

4.1. Scale of measurements

In the present study we measure displacements of points in the micrographs, as the wood specimen is deformed. The displacement data are then transformed to strain data. The measured displacements are obtained by the correlation procedure described in the experimental section. These displacements are obtained as an average over a subimage of a given size. Our micrograph, in other words, is divided into subimages each of which provides one displacement data point. The spatial resolution of the displacement field will be restricted by the size of this subimage. If the subimage is smaller, the spatial resolution increases. However, we run into problems if we reduce the size of the subimage to such an extent that, as an example, it resides entirely within the wall of one cell. A local cell wall may be subjected to large displacements very different from the average continuum displacement we are interested in. For this reason, the subimage size must be large enough to represent the continuum displacement. The choice of subimage size is therefore based on an optimization procedure balancing criteria for continuum representation and spatial resolution.

In the present analysis we used a subimage size of 32×32 pixels ($\simeq 70 \times 70$ μm). This exhibits a smooth deformation field and an acceptable spatial resolution. When the same image was analyzed with a subimage size of 16×16 pixels, large local variations in the deformation field were observed, incompatible with a continuum representation. In order to exclude that this was an effect of erroneous peak location because of insufficient information in the subimage, the same area on the sample was analysed at double magnification with a subimage size of 32×32 pixels. This gave the same local variation in the calculated displacement field as the subimage size 16×16 pixels, which indicates that this is not an effect of erroneous peak location.

4.2. Strain field data

The calculated strain field is given as iso-strain curves printed on top of the micrograph from which it was

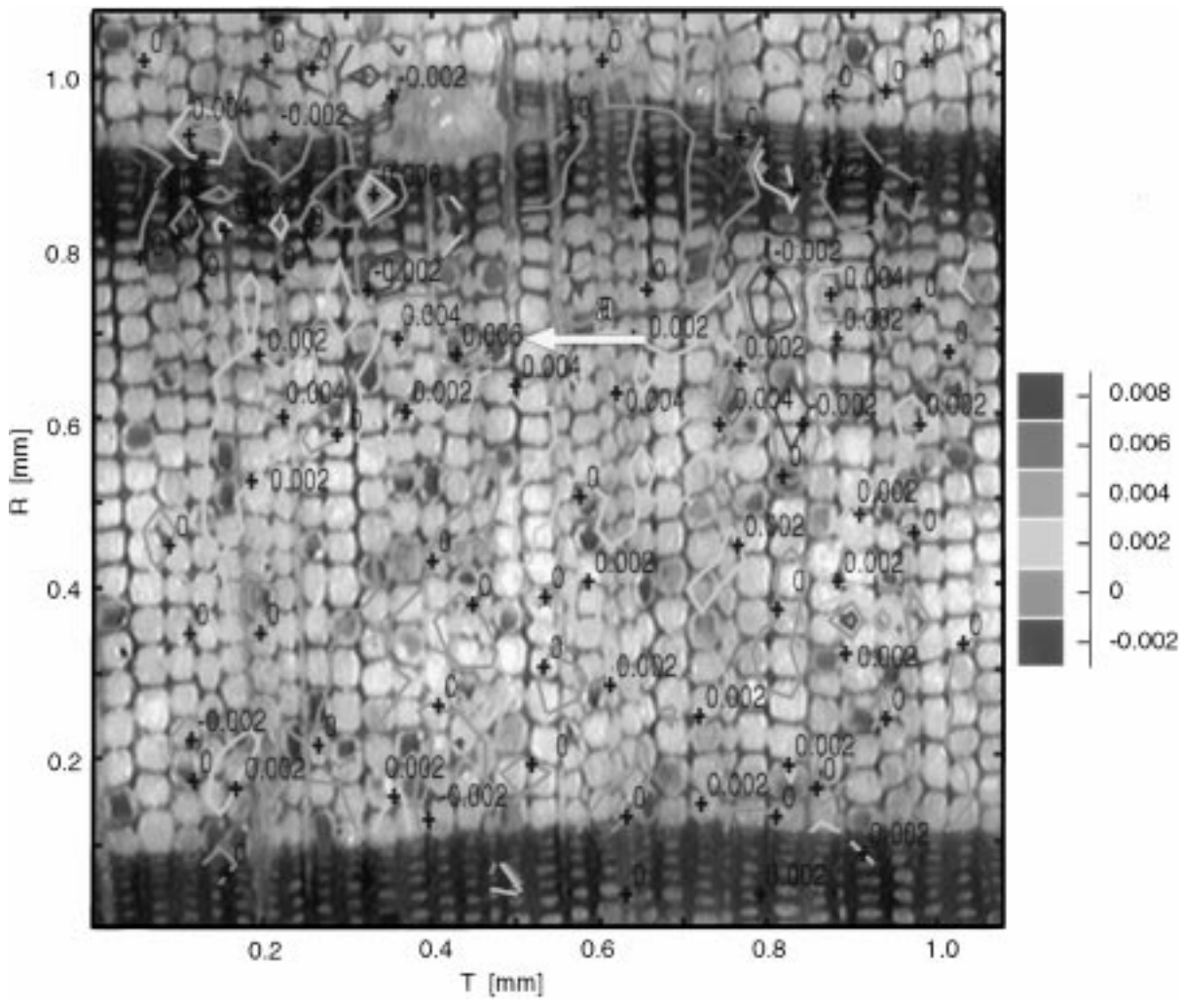

Figure 6 Crack tip at position a: The second load increment. The strain field starts to develop. It extends in the tangential direction close to the latewood layer passed by the crack. The + and the corresponding number (in dimensionless strain) mark the corresponding strain.

calculated. As the cracked specimen is increasingly loaded, the reduced digital image data provide the strain field. The in-plane strain components were calculated by the triangular element method, as described previously. Our data include normal radial strain ε_R, in-plane shear strain ε_{RT} and tangential strain ε_T. Since ε_R and ε_{RT} were found to be low and not very sensitive to increased loading, our discussion is focused on tangential strain ε_T. In Fig. 5, the strain field is plotted in colour code, with the optical micrograph as background. The latewood is apparent as two dark layers where the cells have thicker walls. The earlywood layer inbetween is of fairly uniform density. The density transition at the lower earlywood/latewood interface is dramatic from one row of cells to the next. This is the interface where latewood growth stops in the fall and earlywood growth commences in the spring. At the upper earlywood/latewood interface, a more gradual density transition is discernible, corresponding to the start of latewood growth.

The tip of the crack is located at the tip of the arrow in Fig. 5, the specimen is a compact tension specimen to which increasing load is applied in a tensile test machine (see experimental description). The strain levels are low at this first load increment. One may note some jagged irregularities in the strain field data. This is because of limitations in our spatial resolution of 16 pixels (0.03 mm). At the second incremental increase in load level, the strain field presented in Fig. 6 is obtained. We notice a rapid decrease in strain level in the plane of the crack ($T = 0.5$ mm) as we move away from the crack tip at $R = 0.7$ mm towards $R = 0.4$ mm and lower R–values. However, in the tangential direction the strain field is extended significantly, producing a total strain field very different from that in a material with homogeneous properties. Note that the measured strains are quantitative in the sense that we can determine the actual homogenized strains relative to the reference image.

In Fig. 7, the load level has been increased further. Strains are higher and the size of the strain field is increased. An interesting strain field geometry develops with increasing load. In the plane of the crack ($T = 0.5$ mm), strains decrease rapidly and are low already at $R < 0.4$ mm, only 0.3 mm away from the crack tip. In contrast, in planes to the left ($T = 0.2$ mm) and to the right ($T = 0.7$ mm) of the crack, strains are significant in the range $R = 0.7$ mm to $R = 0.2$ mm.

The shape of the strain field geometry is unusual and obviously a consequence of the large stiffness difference between the earlywood and latewood layers. Note the low strains in the earlywood region close to the

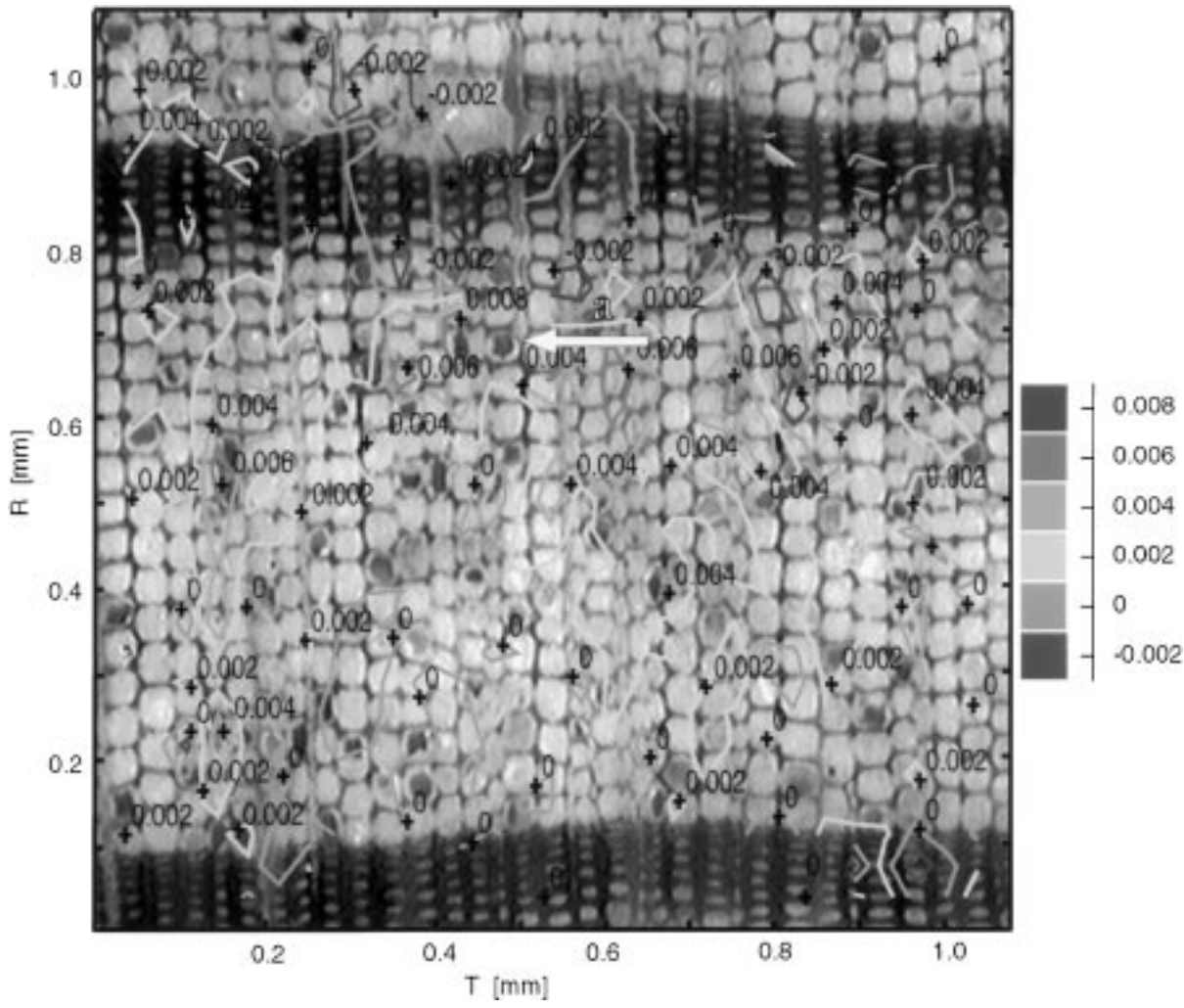

Figure 7 Crack tip at position a: The third load increment. The strain field is further developed and the extension in the tangential direction is enhanced. The + and the corresponding number (in dimensionless strain) mark the corresponding strain.

lower part of the upper latewood layer. This is because of the stiffening effect of the latewood. Finally, the tendency of the strain field to exhibit unsymmetric features is primarily because insufficient data were collected in the very left part of the micrograph. The crack itself is now apparent with a visible crack opening displacement. Strains are small in the stiff latewood regions (dark areas). In the tangential direction (T–direction), high strains are present over a significant range, especially at the y-coordinate ($R \simeq 0.6$ mm) corresponding

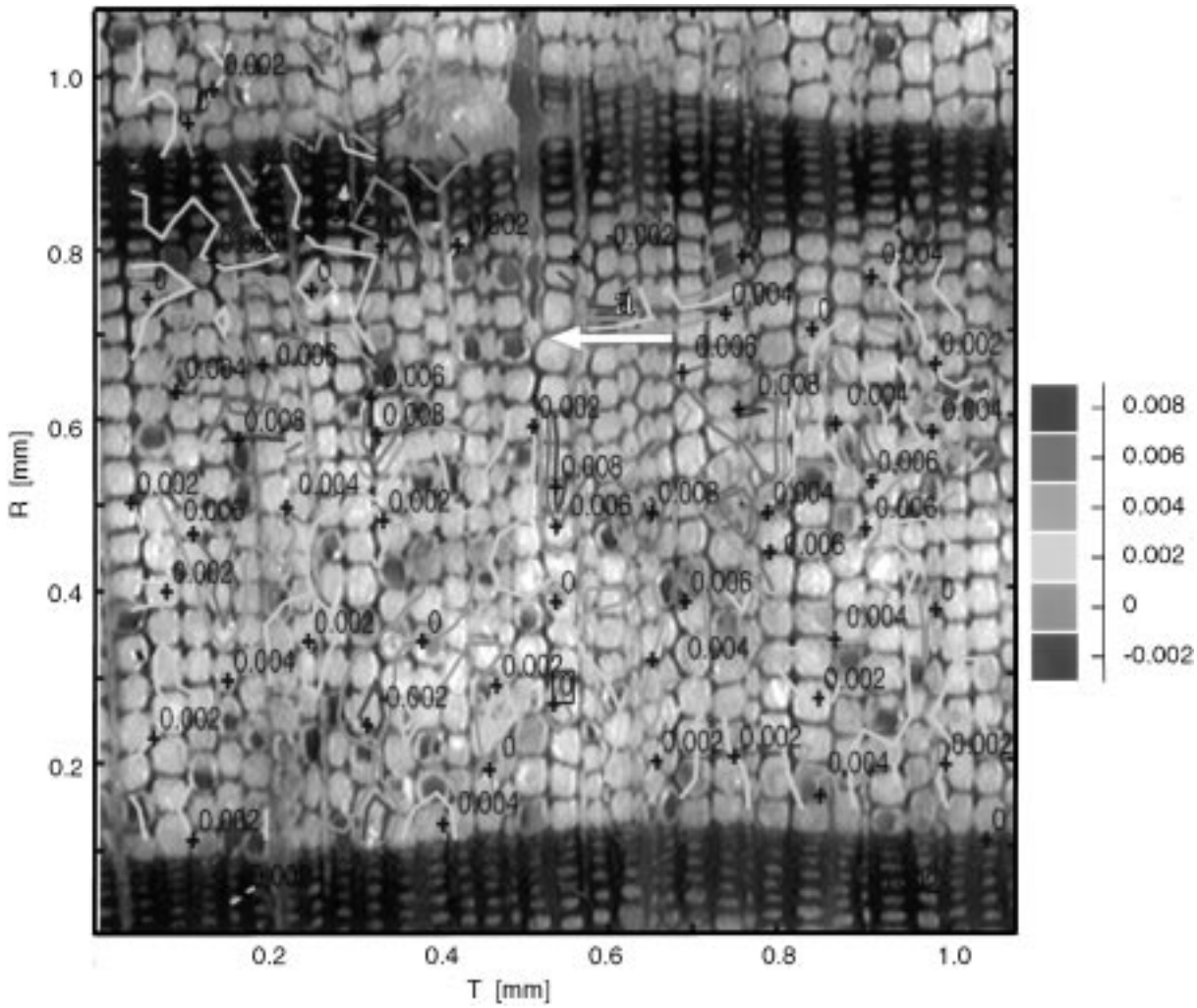

Figure 8 Crack tip at position a: The fourth load increment. The strain field has now developed and reached the upcoming latewood layer. In front of the cracktip, however, there is a local area of small strains close to the upcoming latewood layer. The + and the corresponding number (in dimensionless strain) mark the corresponding strain.

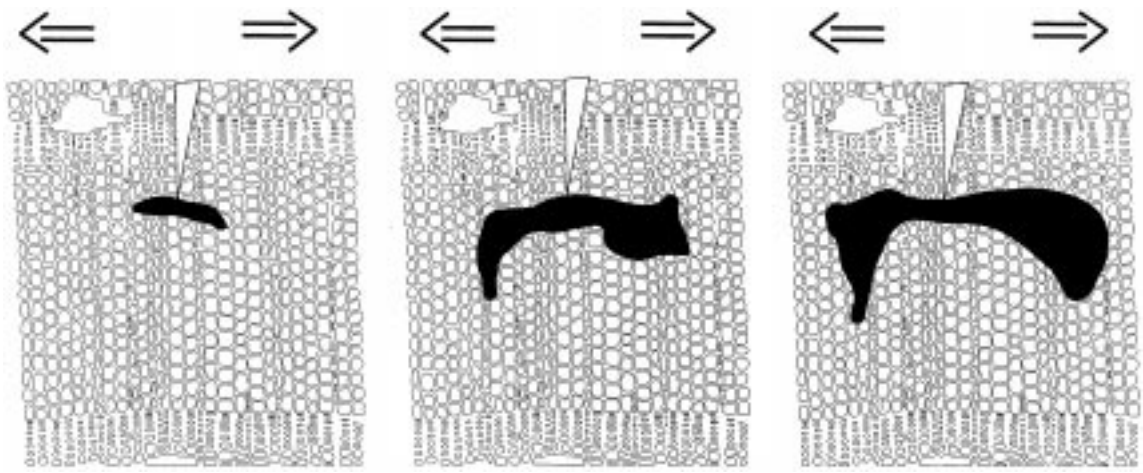

Figure 9 Schematic description of the strain field development with increasing opening mode loading of a preexisting crack. Upper and lower parts of the images correspond to latewood layers.

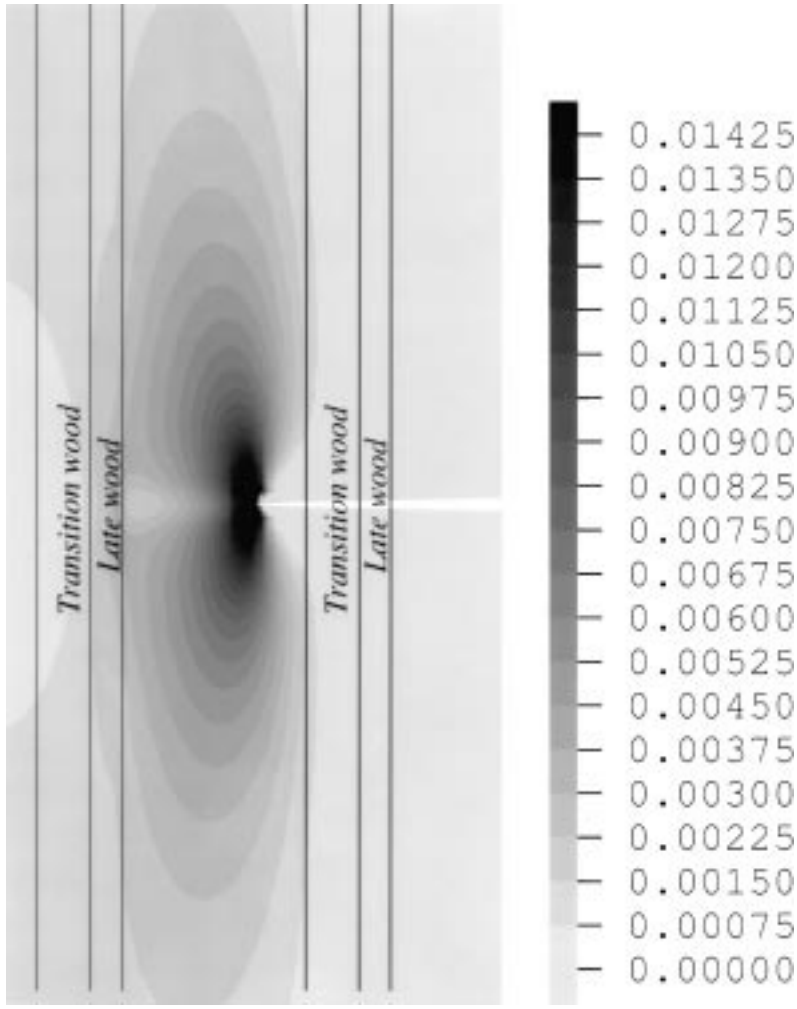

Figure 10 Tangential strain field calculated by FEM [24]. Width of the growth ring, $w = 1.6$ mm.

to the tip of the crack. In the upper right part of the upper latewood layer, no data are given. The reason is that the displacement exceeded the number of pixels in half the subimage size, in this case 16 pixels ($\simeq$0.03 mm), which is the limit set in the correlation algorithm. The information in Fig. 5 to 8 is summarized by the sketch in Fig. 9, where one of the isostrain curvatures is used as a boundary for a large strain area. The strain field extends significantly in the tangential, T, direction, but is constrained in the radial, R, direction. This is particularly true in the plane of the crack.

The tangential modulus of the latewood layers is about 20 times as high as it is in the earlywood. This estimate is based on the elasticity models for cell aggregates given by Gibson and Ashby [22] (the density ratio between latewood and earlywood required as input is about 3 for *Pinus sylvestris* L. [23]). Recently, the *TR* crack considered in the present study was also studied by finite element analysis [24]. Tangential strain field data from that study are presented in Fig. 10. The shape of the calculated strain field correlates well with the measured shape. Strains extend in the tangential direction. In the radial direction, the tangential strain field is constrained by the stiff latewood layer.

From the summary in Fig. 9, it is apparent that as we move from the plane of the crack in the tangential direction, strains extend a bit further in the radial direction. This feature is also predicted by the theoretical analysis.

5. Conclusions

The *TR* crack tip strain field in wood was determined by electronic speckle photography. Strains were measured on direct images of the microstructure, allowing correlation between strain field data and microstructure. Reported data were for the transverse strain field at the level of growth rings. The scale at which the strain field was observed was of crucial importance for the outcome of the experiments. This scale was determined in an optimization process. The error from viewing the material as a continuum was balanced with respect to our ability to observe effects from local microstructural variations.

In the softer earlywood, strains extended considerable distances in the tangential direction. Due to the stiff latewood, the strain was heavily constrained in the radial direction. Inspired by these results, a corresponding theoretical FEM-study has been conducted [24]. These FEM results for the crack tip strain field show good correlation with the present data. The nature of the local strain field at the scale of growth rings has been largely neglected, despite its obvious significance to *TR* crack growth mechanisms.

Acknowledgements

Financial support from SJFR for one of us, Fredrik Thuvander, is gratefully acknowledged.

References

1. T. ENGØY, K. J. MÅLØY, A. HANSEN and S. ROUX, *Phys. Rev. Lett.* **73** (1994) 834.
2. A. P. SCHNIEWIND and R. A. POZNIAK, *Eng. Fract. Mech.* **2** (1971) 223.
3. J. BODIG and B. A. JAYNE, "Mechanics of Wood and Wood Composites" (Van Nostrand Reinhold, New York, 1982).
4. L. A. DONALDSON, *Holzforschung* **51** (1997) 303.
5. J. BODNER, G. GRÜLL and M. G. SCHLAG, *ibid.* **50** (1996) 487.
6. J. BODNER, M. G. SCHLAG and G. GRÜLL, *ibid.* **51** (1997) 479.
7. K. RIIPOLA and M. FONSELIUS, *Journal of Structural Engineering* **118** (1992) 1741.
8. A. P. SCHNIEWIND and J. C. CENTENO, *Wood Fiber Sci.* **5** (1973) 152.
9. D. M. TAN, S. E. STANZL-TSCHEGG and E. K. TSHEGG, *Holz Roh Werkst.* **53** (1995) 159.
10. G. R. DEBAISE, A. W. PORTER and R. E. PENTOENY, *Mater. Res. Stand.* **6** (1966) 493.
11. M. F. ASHBY, K. E. EASTERLING, R. HARRYSSON and S. K. MAITI, *Proc. R. Soc. London A* **398** (1985) 261.
12. F. THUVANDER and L. A. BERGLUND, *J. Mater. Sci.*, Accepted.
13. G. KIFETEW, F. THUVANDER, L. BERGLUND and H. LINDBERG, *Wood Sci. Technol.* **32** (1998) 83.
14. F. THUVANDER, G. KIFETEW and L. A. BERGLUND, *Wood Sci. Technol.*, Accepted.
15. L. BENCKERT, M. JONSSON and N. E. MOLIN, *Opt. Eng.* **26** (1987) 167.
16. A. G. ZINK, R. W. DAVIDSON and R. B. HANNA, *Wood Fiber Sci.* **27** (1995) 346.
17. L. MOTT, S. M. SHALER and L. H. A. GROOM, *ibid.* **28** (1996) 429.
18. M. SJÖDAHL, *Appl. Opt.* **33** (1994) 6667.
19. *Idem., ibid.* **36** (1997) 2875.
20. D. CHOI, J. L. THORPE and R. B. HANNA, *Wood Sci. Technol.* **25** (1991) 251.
21. D. CHOI, J. L. THORPE, W. A. CÔTÉ and R. B. HANNA, *Forest Prod. J.* **6** (1996) 87.
22. L. GIBSON and M. F. ASHBY, "Cellular Solids-Structure and Properties" (Pergamon Press, Oxford, 1988).
23. F. F. P. KOLLMAN and W. A. CÔTÉ, "Principles of Wood Science and Technology" (Springer-Verlag, New York, 1968).
24. F. THUVANDER, L. O. JERNQVIST and J. GUNNARS, *J. Mater. Sci.*, Submitted.

Received 27 July 1998
and accepted 1 February 2000